Batteryless DCM Boost Converter for Kinetic Energy Harvesting Applications

Andrés Gomez-Casseres, Rubén Contreras

Abstract—In this paper, a bidirectional boost converter operated in Discontinuous Conduction Mode (DCM) is presented as a suitable power conditioning circuit for tuning of kinetic energy harvesters without the need of a battery. A nonlinear control scheme, composed by two linear controllers, is used to control the average value of the input current, enabling the synthesization of complex loads. The converter, along with the control system, is validated through SPICE simulations using the LTspice tool. The converter model and the controller transfer functions are derived. From the simulation results, it was found that the input current distortion increases with the introduced phase shift and that, such distortion, is almost entirely present at the zero-crossing point of the input voltage.

Keywords—Average current control, boost converter, electrical tuning, energy harvesting.

I. INTRODUCTION

ENERGY HARVESTING (EH) has played an important role in a huge number of low-power applications, such as: Internet of Things (IoT) [1], [2], Wireless Sensor Networks (WSN) [3], among others, due to the advantages related to the extraction of the energy in the environment, which imply cost and complexity reduction, and the possibility to deploy large amount of nodes without concerning about maintenance issues. Also, the need to obtain information from hard-to-reach environments, has increased the interest in this area.

Although EH presents great advantages in many different engineering scenarios, some challenges, such as the limited bandwidth of the harvesters [4], reduce the output power when the input mechanical force fluctuates [5], making EH applications only suitable for very steady vibration patterns.

Some attempts to increase the bandwidth and power output of kinetic energy harvesters have been made from different areas. For example, the use of nonlinear piezoelectric materials have shown an increase in the harvester bandwidth [6], the implementation of complex structures [7] and electrical tuning, which implements a complex load impedance at the output port of the harvester [4], [8]–[10]. A problem of some of these attempts is the need of batteries, reducing the impact and possible applications of such systems.

In this paper, a batteryless power conditioning system able to perform electrical tuning of kinetic energy harvesters is presented. This system is based on the boost topology. The modeling of the converter and design of the control system is also presented. Verification of the power and control stage is achieved through SPICE simulations.

A. Gomez-Casseres is with the Department of Electronic Engineering, Corporación Unificada Nacional de Educación Superior - CUN, Bogotá, Colombia (e-mail: andres_gomezcasseres@cun.edu.co).
A. Gomez-Casseres and R. Contreras are with Corporación Unificada Nacional de Educación Superior - CUN.
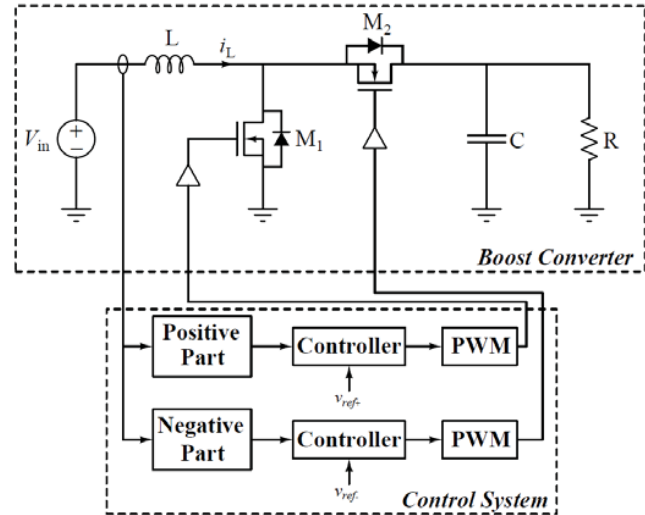
Fig. 1 Power Conditioning System

II. POWER CONDITIONING SYSTEM

The proposed power conditioning system is introduced in Fig. 1, where the schematic of the power converter is shown along with the control system block diagram. The positive and negative part blocks perform a conditioning of the measured current signal, taking only the positive or negative part of the signal, respectively, and passing it to each controller. Each controller compares the measured current signal with a reference (v_{ref+} and v_{ref-}) and, according to the difference of those variables with the averaged current signal, drives a PWM module. Should be noted that each controller takes over the boost converter in different intervals of the current signal, one controls the current for positive values (sinking operation) while the other one for negative values (sourcing operation).

A. System Operation

Given that most kinetic energy harvesters produce a sinusoidal output voltage, a bidirectional current flow is imperative to tune an energy harvester. This functionality is achieved by the proposed converter using the intrinsic body diodes of the MOSFETs M1 and M2 and switching each MOSFET when a specific current direction is desired. When a current direction from the harvester to the load is needed, called as sinking operation, M1 is controlled by one of the PWM blocks while M2 remains off. This operation mode is the normal operation of the boost converter, given that the inductor current is transferred to the load by the intrinsic body diode of M2. Conversely, when a current from the load to the source
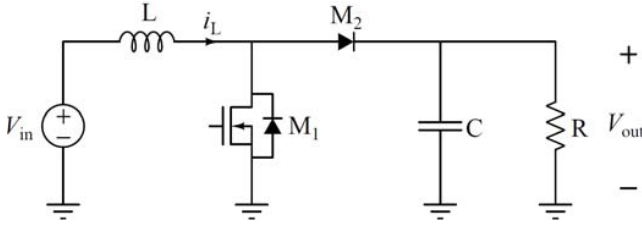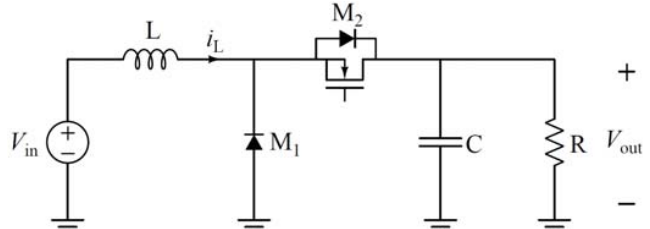
Fig. 2 Converter Under Sinking Operation

Fig. 3 Converter Under Sourcing Operation

is required, M2 is switched and M1 is turned off, allowing its diode to conduct in a portion of the cycle. This is called sourcing operation.

B. Modeling under Sinking Operation

The boost converter, operating in sinking operation (positive inductor current), is shown in Fig. 2. During the interval $0tdT_s$, where d is the duty cycle and T_s is the switching period, M1 is turned on, making the voltage on the inductor equal to the input voltage and the current through the capacitor equal to the load current. During the interval $dT_s < t \leq (d+d_2)T_s$, M1 is off and the body diode of M2 conducts the inductor current. This makes the voltage on the inductor equal to the difference between the input and output voltages, and the current trough the capacitor equal to the inductance current minus the load current. Finally, during the interval $(d + d_2)T_s < t \leq T_s$, the inductor current reaches zero, and the diode of M2 stops conducting.

By averaging the relationships described above, following the method in [11], the model for the boost converter operating in DCM is obtained. This model is presented in (1) and (2).

$$L\frac{di_L}{dt} = \frac{2L}{d^2T_s}di_L\left(1 - \frac{v_{out}}{v_{in}}\right) + dv_{out} \tag{1}$$

$$C\frac{dv_{out}}{dt} = i_L - \frac{d^2T_s}{2L}v_{in} - \frac{v_{out}}{R} \tag{2}$$

The model presented in (1) and (2) is a large-signal nonlinear model. In order to obtain a linear relationship between the input current (i_L) and the duty cycle (d), the jacobian matrix is used. This leads to the linear small-signal state space model presented in (3)-(5).

$$A_{sink} = \begin{bmatrix} \frac{2}{DT_s}\left(1 - \frac{V_{out}}{V_{in}}\right) & \frac{D}{L} - \frac{2I_L}{DT_sV_{in}} \\ \frac{1}{C} & \frac{-1}{RC} \end{bmatrix} \tag{3}$$

$$B_{sink} = \begin{bmatrix} \frac{2}{D^2T_s}\left(I_L + \frac{2I_LV_{out}}{V_{in}} + \frac{D^2T_s}{2L}V_{out}\right) \\ \frac{-DT_s}{LC}V_{in} \end{bmatrix} \tag{4}$$

$$C_{sink} = \begin{bmatrix} 1 & 0 \end{bmatrix} \qquad D_{sink} = 0 \tag{5}$$

Assuming a duty cycle and an input voltage equal to 0.7 and 5 V, respectively, and $R = 10\,\text{k}\Omega$, $C = 4\,\text{mF}$ and $L = 8\,\mu\text{H}$, the evaluation of the matrices in (3) and (4) are presented in (6) and (7). This system, under such conditions, presents two poles at $-11.1091 \cdot 10^6$ rad/s and $-50.321 \cdot 10^{-3}$ rad/s and one zero at -0.05 rad/s.

$$A_{sink} = \begin{bmatrix} -11.1091 \cdot 10^6 & -1.125 \cdot 10^3 \\ 250 & -25 \cdot 10^{-3} \end{bmatrix} \tag{6}$$

$$B_{sink} = \begin{bmatrix} 98.455 \cdot 10^6 \\ -2.187 \cdot 10^3 \end{bmatrix} \tag{7}$$

C. Model under Sourcing Operation

The converter under sourcing operation (negative inductor current) is presented in Fig. 3. The operation under this mode differs from the sinking mode only in the input and output ports. Therefore, the inductor voltages and capacitor currents are the same but appear at different times inside the switching period. For example, during the interval $0 \leq t \leq dT_s$, M2 is turned on, making the voltage on the inductor equal to the difference between the input and output voltages, instead of being equal to the input voltage.

Under this mode of operation, the converter presents the large signal model shown in (8) and (9). Given that the current would be obtained from the stored charge in the capacitor, the system does not have a different equilibrium point than zero. Therefore, an output voltage equal to 6 V is assumed. This leads to the small signal model presented in (10)-(12).

$$L\frac{di_L}{dt} = \frac{2L}{dT_s}\frac{i_Lv_{in}}{v_{in} - v_{out}} + dv_{out} \tag{8}$$

$$C\frac{dv_{out}}{dt} = \frac{d^2T_s}{2L}(v_{in} - v_{out}) - \frac{v_{out}}{R} \tag{9}$$

$$A_{source} = \begin{bmatrix} -714.28 \cdot 10^3 & -612.5 \cdot 10^3 \\ 0 & -153.15 \end{bmatrix} \tag{10}$$

$$B_{source} = \begin{bmatrix} -1.5 \cdot 10^6 \\ -437.5 \end{bmatrix} \tag{11}$$

$$C_{source} = \begin{bmatrix} 1 & 0 \end{bmatrix} \qquad D_{source} = 0 \tag{12}$$

The system shown in (10)-(12) presents two poles locatet at $-714.285 \cdot 10^3$ and -153.15. Also, the system has a Right Half Plane Zero (RHPZ) ubicated at 25.49. This RHPZ is due to the discharge of the output capacitor during sourcing operation and, in terms of the control design, limits the bandwidth of the control loop and presents and undershoot in the step response of the system [12].

In order to avoid the problems presented by the RHPZ, the assumption that the output voltage does not have a significant change is used. This implies that the output capacitor must

TABLE I
CONTROLLER PARAMETERS

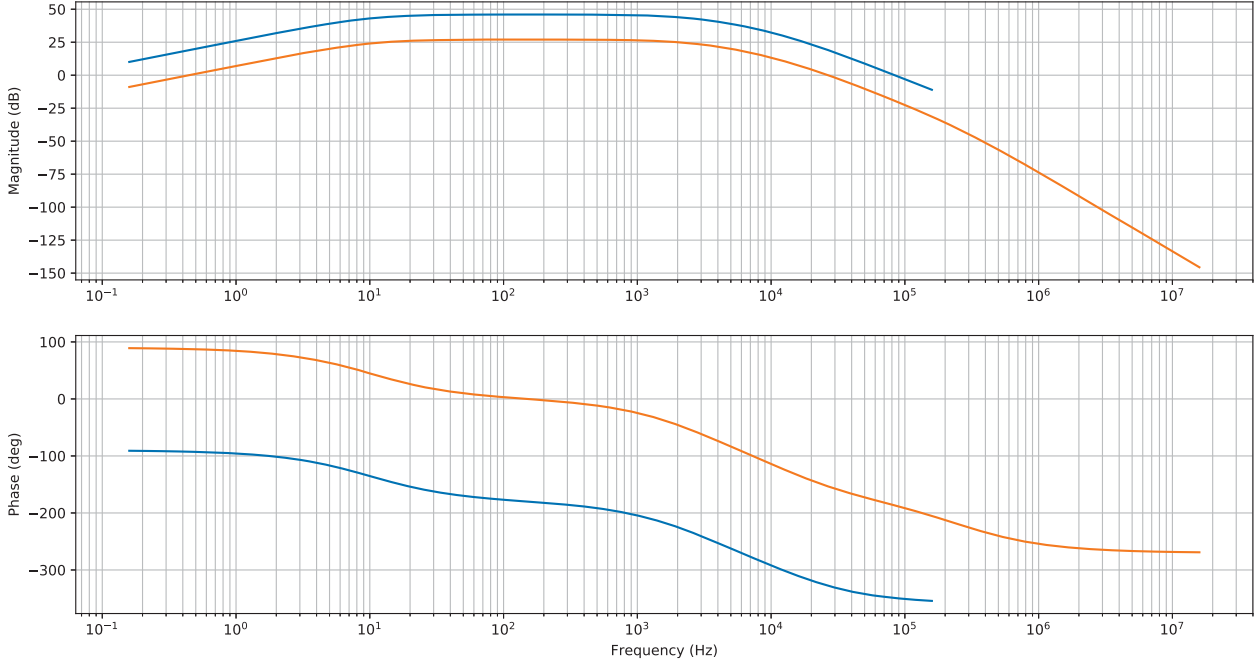|	G_{c0}	ω_{p1}	ω_{p2}	ω_{p3}
Sinking Controller	50	16053.532 rad/s	80120.13 rad/s	62.831 rad/s
Sourcing Controller	−200	16792.181 rad/s	83676.24 rad/s	62.832 rad/s

Fig. 4 Controllers bode plot: Controller for sinking operation (orange) and controller for sourcing operation (blue)

be large enough and the current given to the source must be small, which, in most of the energy harvesting applications, holds for the time when the sourcing operation is maintained. The use of this approximation, and the previous parameters, lead to the model shown in (13), which neglects the dynamics of the output port of the system.

$$A_{source} = \begin{bmatrix} -714.28 \cdot 10^3 \end{bmatrix} \quad B_{source} = \begin{bmatrix} -1.5 \cdot 10^6 \end{bmatrix} \quad (13)$$

III. CONTROLLER DESIGN

The controllers needed to maintain operation of the converter are designed using frequency domain techniques. Given that the converter is built to operate as an energy harvester, which must extract the maximum power available from a mechanical system, the converter must be able to follow AC current signals between 10 Hz and 1 kHz of frequency. Therefore, average current control and a loop gain crossover frequency of 10 kHz is selected. Furthermore, and with the aim to maintain a fast system response and low overshoot, a Q equal to 0.7 is also selected. A current sensor and PWM gain are selected to be 0.5 kΩ (R_f) and 0.25, respectively.

From the previous parameters, the selected transfer function for the controllers in sinking and sourcing operation is presented in (14). Also, the bode plots of both controllers are presented in Fig. 4, where the controller parameters are

presented in Table I. Should be noted that the main difference between the controllers is the sign of the mid-band gain (G_{c0}).

$$G_c = G_{c0} \frac{1}{\left(1 + \frac{s}{\omega_{p1}}\right)\left(1 + \frac{s}{\omega_{p2}}\right)\left(1 + \frac{\omega_{p3}}{s}\right)} \quad (14)$$

IV. RESULTS

The boost converter, along with the control system, was simulated using the Ltspice tool from Linear Technology. A NVC rectifier [13], [14] is placed between the source and the input port of the converter. The effect of such circuit was not taken into account in the derivation of the reference current waveforms.

The system was tested with a 5 V DC input source and with a 5 V amplitude, 1 kHz sine wave. A 50 kHz switching frequency was selected. Under both conditions, a reference voltage ($R_f\, i_{ref}$) with a 5 mV amplitude and 1 kHz frequency was applied to the control system. In order to test if the system was able to perform a synthesization of complex loads, a phase shift of −30, −60 and −90 degrees was introduced within the voltage reference. Furthermore, the initial condition for the output capacitor was set to 10 V, thus neglecting the start-up CCM dynamics of the converter.

The results from the system simulation are presented in figure, where the waveforms of the instantaneous and averaged input current are presented. Furthermore, the computation
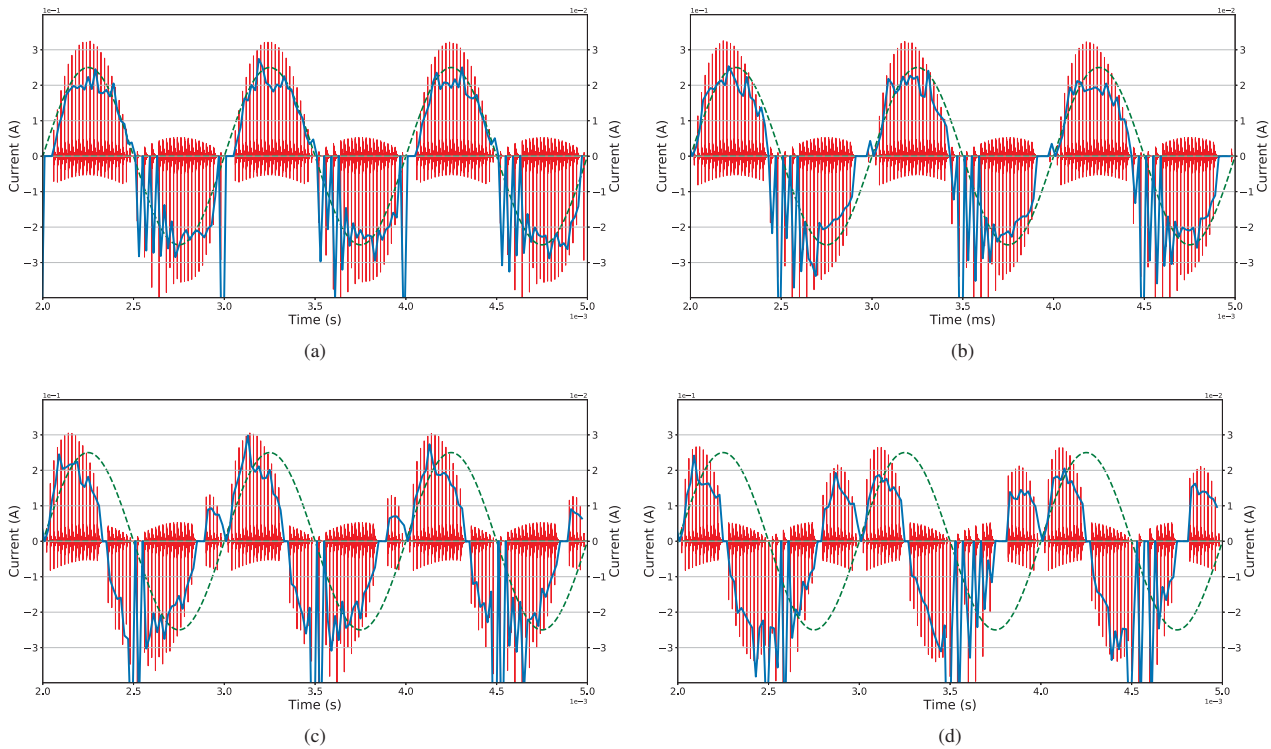
Fig. 5 Simulation results for (a) 0 degrees phase shift, (b) 30 degrees phase shift, (c) 60 degrees phase shift and (d) 90 degrees phase shift

TABLE II
THD COMPUTATION

Phase Shift	THD
0°	491.53 %
30°	521.78 %
60°	575.39 %
90°	539 %

of the *Total Harmonic Distortion* (THD) of the averaged input current waveforms was computed, and is presented in and Table I. In figure, the red waveform is the simulated inductor current, the blue waveform is the average of the inductor current along each switching period and the green dashed waveform is the input voltage. This green waveform was presented as a reference with the aim to visualize the introduced phase shift. Should be noted that the axis corresponding to the red waveform are placed at the left part of Figs. 5a-5d, while the ones related to the blue waveform are placed on the right part of the figures. It is evident, from Figs. 5b-5d and Table I that, as the phase shift increases, the distortion of the averaged inductor waveform also increases. This distortion is mainly present when the voltage waveform crosses 0 V. However, the phase shift between the input voltage and the inductor current is clearly established. This distortion, and a higher converter bandwidth, might be achieved by using CPM converter operation.

V. CONCLUSION

In this paper, a bidirectional boost converter was presented as a power conditioning system for batteryless energy harvesting applications. Additionally, the following of a reference by the average inductor current (input current of the converter) was achieved using a control system composed by two linear controllers. The system was corroborated using spice simulation. It was found that, as the phase shift is increased in the reference current, the distortion of the averaged current waveform also increases. It is found that this distortion appears mostly when the input voltage change its polarity.

REFERENCES

[1] K. Tashiro, "Possibility of magnetic energy harvesting for zero-power sensor," *IEEJ Transactions on Fundamentals and Materials*, vol. 137, no. 8, pp. 442–447, 2017.

[2] G. Venkatesh, "Semiconductor solutions for the internet of things: The role of event detection, asynchronous design, energy harvesting and flexible electronics," *Journal of the Indian Institute of Science*, vol. 93, no. 3, pp. 441–461, 2013.

[3] A. Sanchez Ramirez, K. Das, R. Loendersloot, T. Tinga, and P. Havinga, "Wireless sensor network for helicopter rotor blade vibration monitoring: Requirements definition and technological aspects," *Key Engineering Materials*, vol. 569, pp. 775–782, 2013. (Online). Available: http://doc.utwente.nl/87397/.

[4] J. A. Bowden, S. G. Burrow, A. Cammarano, L. R. Clare, and P. D. Mitcheson, "Switched-Mode Load Impedance Synthesis to Parametrically Tune Electromagnetic Vibration Energy Harvesters," *IEEE-ASME Transactions on Mechatronics*, vol. 20, no. 2, pp. 603–610, 2015.

[5] A. R. M. Siddique, S. Mahmud, and B. Van Heyst, "A comprehensive review on vibration based micro power generators using electromagnetic and piezoelectric transducer mechanisms," *Energy Conversion and Management*, vol. 106, pp. 728–747, 2015.

[6] S. P. Beeby, L. Wang, D. Zhu, A. S. Weddell, G. V. Merrett, B. Stark, G. Szarka, and B. M. Al-Hashimi, "A comparison of power output from linear and nonlinear kinetic energy harvesters using real vibration data," *Smart Materials and Structures*, vol. 22, no. 7, p. 075022, 2013.

[7] S. G. Burrow and L. Penrose, "A 2 DOF vibration harvester for broadband and multifrequency harvesting using a single electro-magnetic transducer," *Journal of Physics: Conference Series*, vol. 557, no. 1, p. 12031, 2014.

[8] A. Cammarano, S. G. Burrow, D. A. W. Barton, A. Carrella, and L. R. Clare, "Tuning a resonant energy harvester using a generalized electrical load," *Smart Materials and Structures*, vol. 19, no. 5, may 2010.

[9] S. Saggini, S. Giro, F. Ongaro, and P. Mattavelli, "Implementation of reactive and resistive load matching for optimal energy harvesting from piezoelectric generators," *2010 IEEE 12th Workshop on Control and Modeling for Power Electronics (COMPEL)*, pp. 1–6, 2010.

[10] G. D. Szarka, B. H. Stark, and S. G. Burrow, "Review of Power Conditioning for Kinetic Energy Harvesting Systems," *IEEE Transactions on Power Electronics*, vol. 27, no. 2, pp. 803–815, feb 2012.

[11] J. Sun, D. M. Mitchell, M. F. Greuel, P. T. Krein, and R. M. Bass, "Averaged modeling of PWM converters operating in discontinuous conduction mode," *Power Electronics, IEEE Transactions on*, vol. 16, no. 4, pp. 482–492, jul 2001.

[12] J. B. Hoagg and D. S. Bernstein, "Nonminimum-phase zeros - Much to do about nothing," *IEEE Control Systems Magazine*, vol. 27, no. 3, pp. 45–57, jun 2007.

[13] C. Peters, J. Handwerker, D. Maurath, and Y. Manoli, "A Sub-500 mV Highly Efficient Active Rectifier for Energy Harvesting Applications," *IEEE Transactions on Circuits and Systems I: Regular Papers*, vol. 58, no. 7, pp. 1542–1550, jul 2011.

[14] E. A. Gomez-Casseres, S. M. Arbulu, R. J. Franco, R. Contreras, and J. Martinez, "Comparison of passive rectifier circuits for energy harvesting applications," in *Canadian Conference on Electrical and Computer Engineering*, vol. 2016-Octob, 2016.